Electronic Supplementary Information

Tuning the membrane permeability of polymersome nanoreactors developed by aqueous emulsion polymerization-induced self-assembly

Spyridon Varlas,[a] *Jeffrey C. Foster,*[a] *Panagiotis G. Georgiou,*[a,b] *Robert Keogh,*[a,b] *Jonathan T. Husband,*[a] *David S. Williams,*[a,c] *and Rachel K. O'Reilly*[a]*

[a] School of Chemistry, University of Birmingham, B15 2TT, Birmingham, UK

[b] Department of Chemistry, University of Warwick, Gibbet Hill Road, CV4 7AL, Coventry, UK

[c] Department of Chemistry, College of Science, Swansea University, SA2 8PP, Swansea, UK

*Corresponding Author: r.oreilly@bham.ac.uk (R.K.O.R.)

Contents

Experimental Section

Materials and Methods

Materials

Poly(ethylene glycol) methyl ether (average M_n = 5,000 g mol^{-1}, PEG-OH), carbon disulfide (anhydrous, ≥99%), sodium ethanethiolate, *N,N′*-dicyclohexylcarbodiimide (99%, DCC), 4-(dimethylamino)pyridine (≥98%, DMAP), benzylamine (99%, BA), 1-naphthylmethylamine (97%, NMA), ethylenediamine (≥99%, C_2DA), 1,3-diaminopropane (≥99%, C_3DA), 1,4-diaminobutane (99%, C_4DA), hexamethylenediamine (98%, C_6DA), poly(ethylene glycol) diamine (average M_n = 2,000 g mol^{-1}), glycidol (96%) and 3,3′-dimethoxybenzidine (DMB) were purchased from Sigma Aldrich and were used without further purification. Glycidyl methacrylate (97%, GlyMA) was also purchased from Sigma-Aldrich and was passed through a column of basic alumina to remove inhibitor prior to use. Iodine, diethyl ether and dichloromethane (DCM) were purchased from Fisher Scientific. 4,4'-Azobis(4-cyanovaleric acid) (98%, ACVA) and poly(ethylene glycol) diamine (average M_n = 1,000 g mol^{-1}) were obtained from Alfa Aesar. 2-Hydroxypropyl methacrylate (mixture of isomers, 98%, HPMA) was also purchased from Alfa Aesar and was passed through a column of basic alumina to remove inhibitor prior to use. 1-Adamantanemethylamine (98%, AMA) was purchased from Acros Organics. *p*-Xylylenediamine (>99.0%, PXDA) was obtained from Tokyo Chemical Industry UK. Hydrogen peroxide (35%) was purchased from Lancaster Synthesis. The enzyme peroxidase from *Amoracia rusticana* (type VI, essentially salt free) (HRP) was purchased from Sigma Aldrich, divided into aliquots at 200 U mL^{-1} in deionized water and stored at -20 °C. Nunc™ 96-well microplates were purchased from ThermoFisher Scientific. Formvar and lacey-carbon coated copper grids were purchased from EM Resolutions.

Characterization Techniques

NMR Spectroscopy. ^{1}H-NMR and ^{13}C-NMR spectra were recorded at a 400 MHz on a Bruker DPX-400 spectrometer, with chloroform-*d* ($CDCl_3$) or methanol-d_4 (CD_3OD) as the solvent. Chemical shifts of protons are reported as δ in parts per million (ppm) and are relative to tetramethylsilane (TMS) at δ = 0 ppm when using $CDCl_3$ or solvent residual peak (CH_3OH, δ = 3.31 ppm).

FT-IR Spectroscopy. Fourier Transform-Infrared (FT-IR) spectroscopy measurements were carried out using an Agilent Cary 630 FT-IR spectrometer, in the range of 650 to 4000 cm^{-1}, after lyophilization of an aliquot of sample.

Size Exclusion Chromatography. Size exclusion chromatography (SEC) analysis was performed on a system composed of a Varian 390-LC-Multi detector suite equipped with a Varian Polymer Laboratories guard column (PLGel 5 μM, 50 × 7.5 mm), two Mixed-C Varian Polymer Laboratories columns (PLGel 5 μM, 300 × 7.5 mm) and a PLAST RT auto-sampler. Detection was conducted using a differential refractive index (RI) and an ultraviolet (UV) detector set to λ = 309 nm. The mobile phase used was DMF (HPLC grade) containing 5 mM NH_4BF_4 at 50 °C at flow rate of 1.0 mL min^{-1}. Poly(methyl methacrylate) (PMMA) standards were used for calibration. Number average molecular weights (M_n), weight average molecular weights (M_w) and dispersities ($Đ_M = M_w/M_n$) were determined using Cirrus v3.3 SEC software.

High-Performance Liquid Chromatography. Reverse phase high-pressure liquid chromatography (RP-HPLC) was carried out using a Shim-pack GISS 5 μm C18 (4.6 × 125 mm) column on a Shimadzu instrument using the following modules: LC-20AD solvent delivery module, SIL-20AC HT autosampler, CTO-20AC column oven and SPD-M20A photodiode array UV-Vis detector. The 222 nm peptide bond absorbance was extracted from the PDA detector. The mobile phases used were H_2O (18.2 MΩ·cm + 0.04% v/v formic acid)/MeCN (HPLC grade + 0.04% v/v formic acid). A range of mobile phase gradients was investigated. The optimized gradient was ran at 0.8 mL min^{-1} at 30 °C and is shown in Table S1.

Table S1. Mobile phase composition used for HPLC analysis.

Time (min)	% H_2O	% MeCN
0	95	5
3	80	20
16	25	75
20	5	95
21	95	5
25	95	5

Matrix-Assisted Laser Desorption/Ionization Time-of-Flight Mass Spectrometry. MALDI-ToF MS was conducted on a Bruker Ultraflex MALDI TOF/TOF mass spectrometer. A solution of HRP (0.2 mg ml^{-1}) was spotted onto a 96-spot steel plate followed by an equal volume of sinapic acid matrix (15 mg in 0.5 mL of water, 0.5 mL of acetonitrile and 1 μL of trifluoroacetic acid (TFA)). The solvent was evaporated before the recording of spectra and analysis using flexControl software.

Dynamic Light Scattering. Hydrodynamic diameters (D_h) and size distributions of particles were determined by dynamic light scattering (DLS) using a Malvern Zetasizer Nano ZS with a 4 mW He-Ne 633 nm laser module operating at 25 °C. Measurements were carried out at an angle of 173° (back scattering), and results were analyzed using Malvern DTS 7.03 software. All determinations were repeated 5 times with at least 10 measurements recorded for each run. D_h values were calculated using the Stokes-Einstein equation where particles are assumed to be spherical.

Zeta Potential Analysis. Zeta potential was measured by the technique of microelectrophoresis, using a Malvern Zetasizer Nano ZS instrument, at room temperature at 633 nm. All reported measurements were the average of at least five runs. Zeta potential was calculated from the corresponding electrophoretic mobilities (μ_E) by using the Henry's correction of the Smoluchowski equation ($\mu_E = 4\pi\ \varepsilon_0\ \varepsilon_r\ \zeta\ (1+\kappa r)/6\pi\ \mu$).

Optical Microscopy. Images of the monomer-in-water emulsion solution prior to polymerization were captured using a Leica DM IL LED optical microscope equipped with a Leica MC170 HD colour camera at 10× magnification. 10 μL of the freshly prepared sample was added on a glass slide and imaged within 5 min after emulsion formation.

Transmission Electron Microscopy. Dry-state stained TEM imaging was performed on either a JEOL JEM-2000 FX or a JEOL JEM-2100Plus microscope operating at an acceleration voltage of 200 kV and a JEOL JEM-1400 microscope operating at an acceleration voltage of 80 kV. All dry-state samples were diluted with deionized water and then deposited onto formvar-coated copper grids. After roughly 1 min, excess sample was blotted from the grid and the grid was stained with an aqueous 1 wt% uranyl acetate (UA) solution for 1 min prior to blotting, drying and microscopic analysis.

Cryogenic transmission electron microscopy (cryo-TEM) imaging was performed on a JEOL JEM-2100Plus microscope operating at an acceleration voltage of 200 kV. Samples for cryo-TEM imaging were prepared at 0.5% w/w solids content in deionized water by depositing 8 μL sample onto plasma-

treated lacey-carbon coated grids followed by blotting for approximately 5 s and plunging into a pool of liquid ethane, cooled using liquid nitrogen, to vitrify the samples. Transfer into a pre-cooled cryo-TEM holder was performed under liquid nitrogen temperatures prior to microscopic analysis. For the determination of average size and membrane thickness of the vesicles at least 100 particles were analyzed in each case.

Kinetic Colorimetric Analysis. Kinetic colorimetric analysis was performed in 96-well Nunclon™ plates and measured on a BMG Labtech FLUOstar OPTIMA plate reader running in absorbance mode with a filter of $\lambda = 492$ nm. Absorbance values at this wavelength were measured every minute for a period of 30 min. All measurements were performed in at least triplicate.

Photoreactor Setup Specifications

The LED source for the visible-light initiated PISA reactions (TruOpto OSV5X3CAC1E, 4.5 W) was purchased from Rapid Electronics and had a radiant flux of 800 mW@400 mA at 12V DC operating at a wavelength of 400–410 nm. This was fitted to a custom-built setup equipped with a dimmer switch for controlling the output light intensity. The vial base is located 19 mm above the light source to limit heating which creates a 40° cone of light from the center of the LED giving 76% intensity at the perimeter of the sample. In the present study, all photo-PISA reactions were carried out at full output light intensity.

Figure S1. Digital photographs of photoreactor system used in the present study to carry out photo-PISA reactions under 405 nm irradiation.

Supplementary Characterization Data

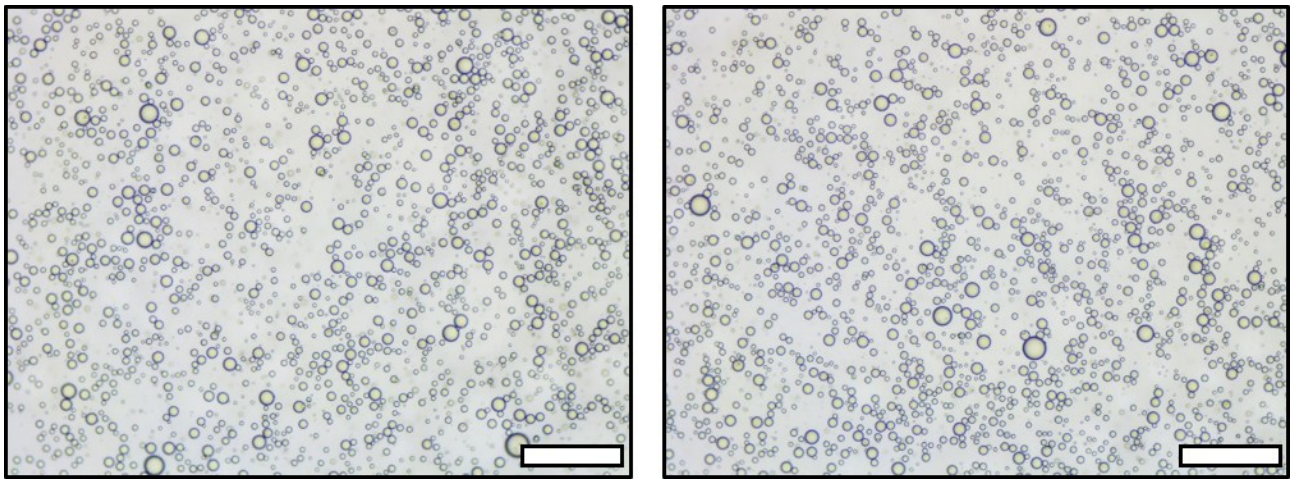

Figure S2. Representative optical microscopy images of initial monomer-in-water emulsion stabilized by PEG_{113} macro-CTA prior to photo-PISA. Scale bars represent 200 μm.

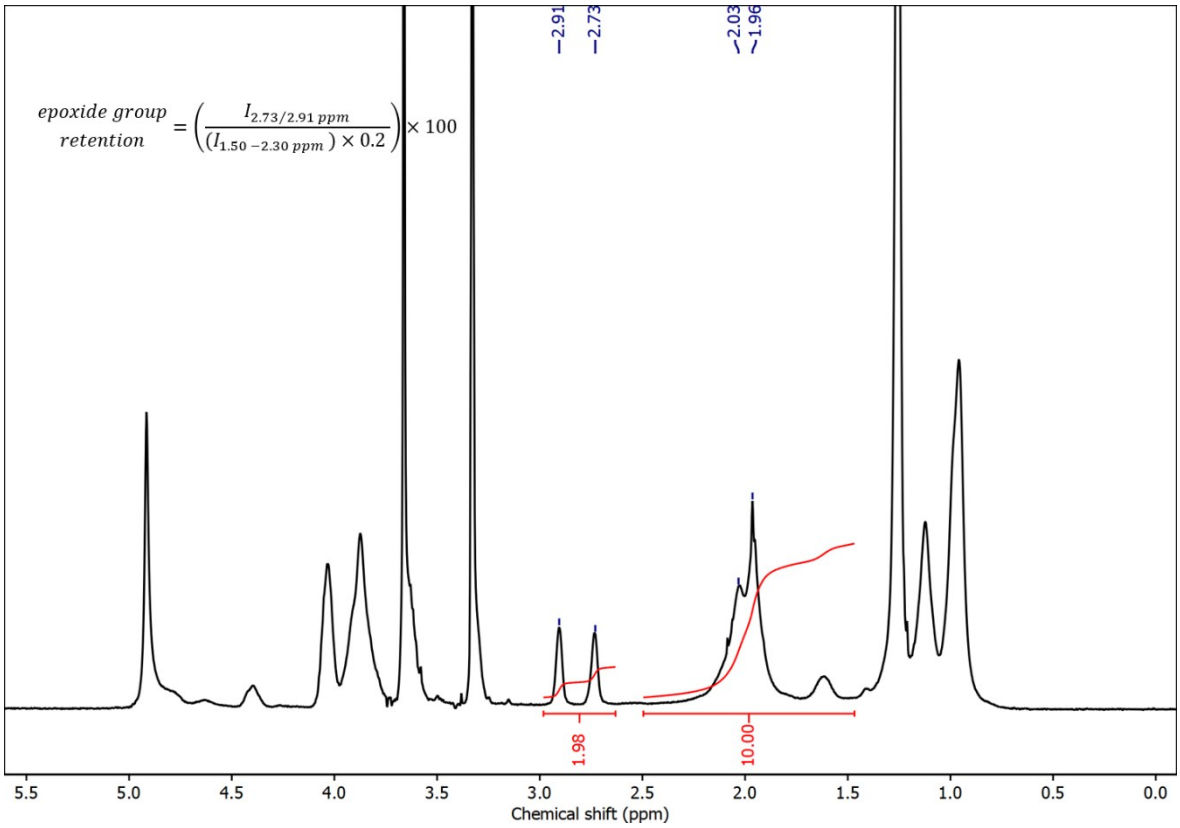

Figure S3. ^{1}H-NMR spectrum of crude PEG_{113}-*b*-P($HPMA_{320}$-*co*-$GlyMA_{80}$) diblock copolymer in methanol-d_4 for calculation of epoxide group retention efficiency after aqueous RAFT-mediated emulsion photo-PISA.

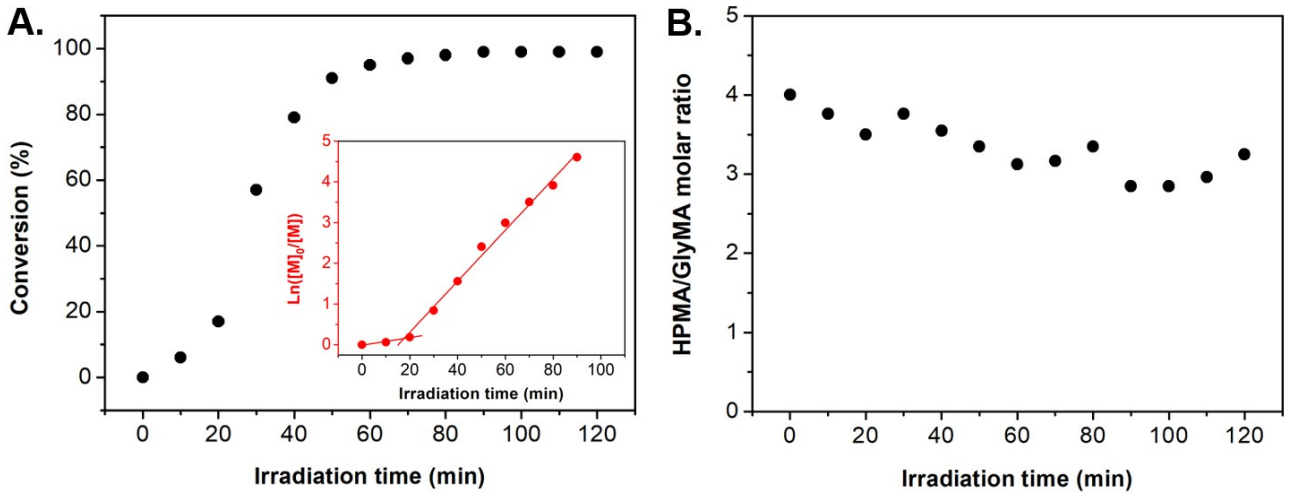

Figure S4. (A) Polymerization kinetics for aqueous RAFT-mediated emulsion photo-PISA of HPMA/GlyMA (80:20 molar ratio) using a PEG_{113} macro-CTA at [solids] = 10% w/w (target DP_{PHPMA} = 320 and DP_{PGlyMA} = 80) (inset: $ln([M]_0/[M])$ versus irradiation time kinetic plot). (B) Relative HPMA/GlyMA monomer molar ratio as a function of photo-PISA irradiation time, as calculated by conversion ^{1}H-NMR analysis in methanol-d_4.

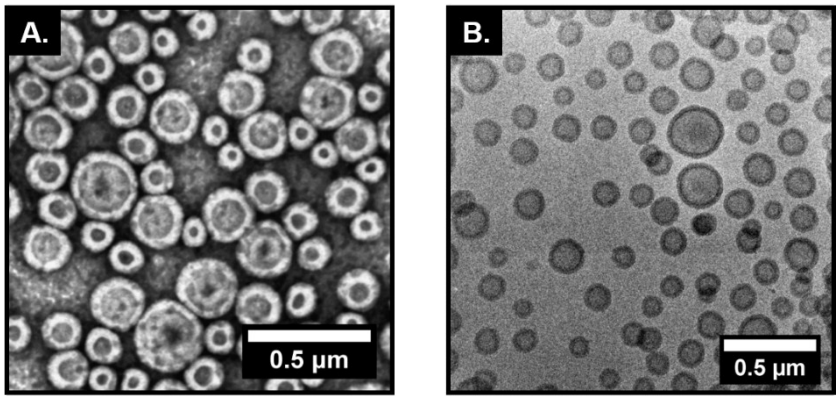

Figure S5. (A) Representative dry-state TEM image, stained with 1 wt% uranyl acetate (UA) solution, and (B) representative cryo-TEM image of empty PEG_{113}-*b*-P($HPMA_{320}$-*co*-$GlyMA_{80}$) vesicles.

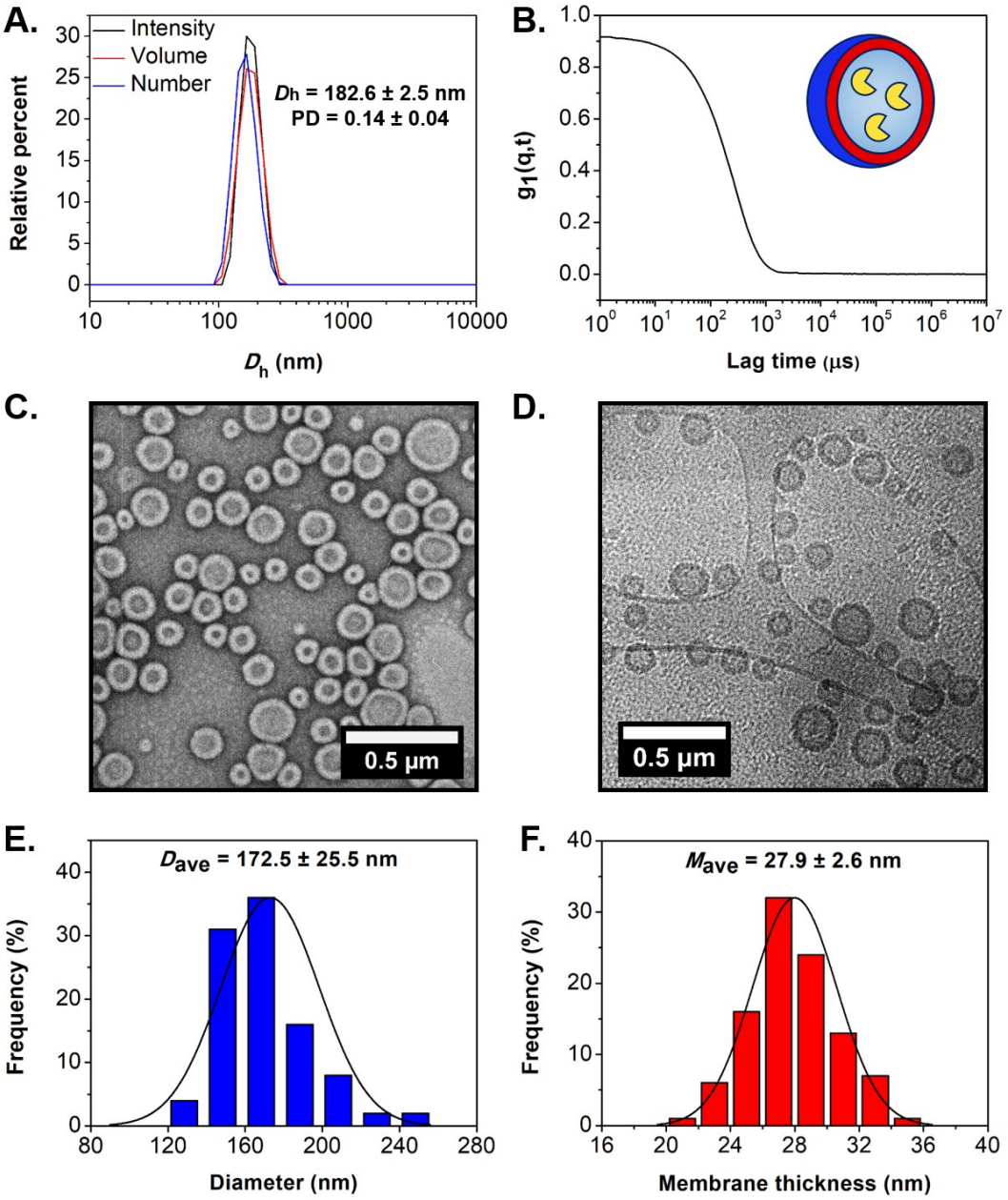

Figure S6. Characterization of purified HRP-loaded PEG_{113}-*b*-P($HPMA_{320}$-*co*-$GlyMA_{80}$) vesicles. (A) Intensity-weighted size distributions along with average D_h and PD values (the error shows the standard deviation from 5 repeat measurements), and (B) autocorrelation function obtained by DLS. (C) Representative dry-state TEM image, stained with 1 wt% UA solution, and (D) representative cryo-TEM image. (E) Histogram of size distribution, and (F) histogram of membrane thickness distribution along with calculated average diameter and membrane thickness values, respectively, measured from particle analysis based on cryo-TEM images. In each case, at least 100 particles were analyzed.

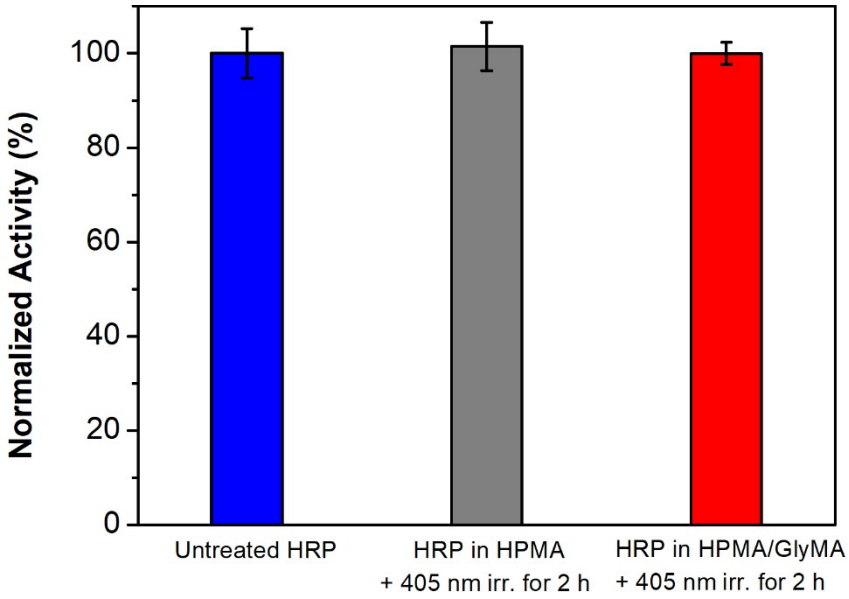

Figure S7. Control experiments comparing the activity of free HRP after incubation at 37 °C for 2 hours under 405 nm irradiation in either 10% w/w HPMA solution in DI water or 10% w/w HPMA/GlyMA (80:20 molar ratio) solution in DI water against untreated enzyme ($[HRP]_{reaction}$ = 20 U mL^{-1}), as determined at the end point of the colorimetric assay (end point = 30 min, λ = 492 nm), showing no loss of HRP activity under aqueous emulsion photo-PISA conditions.

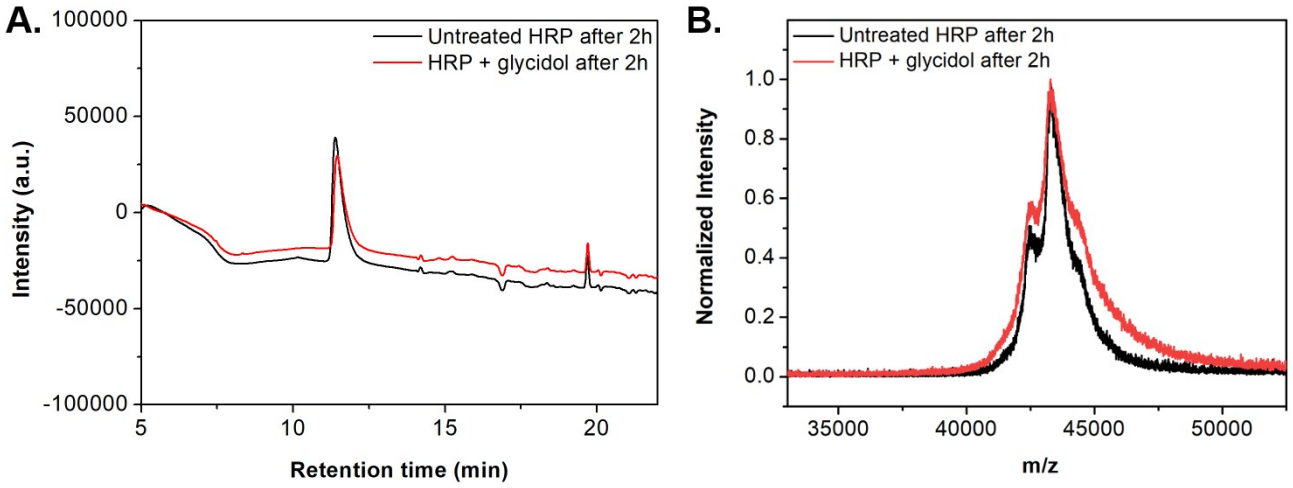

Figure S8. (A) HPLC traces and (B) MALDI-ToF mass spectra of untreated HRP (black traces) and HRP after reaction with water-soluble glycidol (0.14 mmol mL^{-1}) for 2 hours in DI water (red traces) ($[HRP]_{reaction}$ = 20 U mL^{-1}), showing no apparent modification of HRP by ring-opening of the epoxide groups *via* its lysine residues.

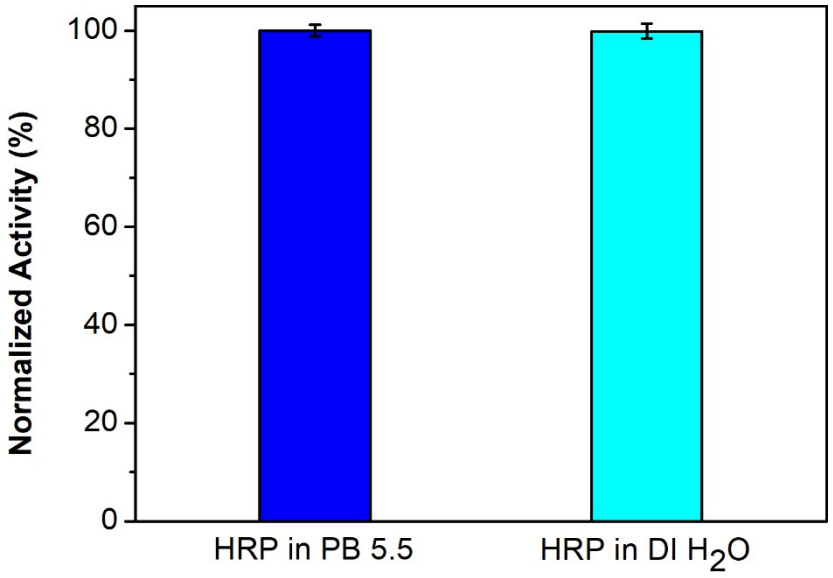

Figure S9. Control experiment comparing the activity of free HRP after incubation at room temperature for 18 hours in either PB 5.5 (optimum pH value of the enzyme) or DI water ($[HRP]_{reaction}$ = 2 U mL^{-1}), as determined at the end point of the colorimetric assay (end point = 30 min, λ = 492 nm), showing no loss of HRP activity under the epoxide ring-opening reaction conditions.

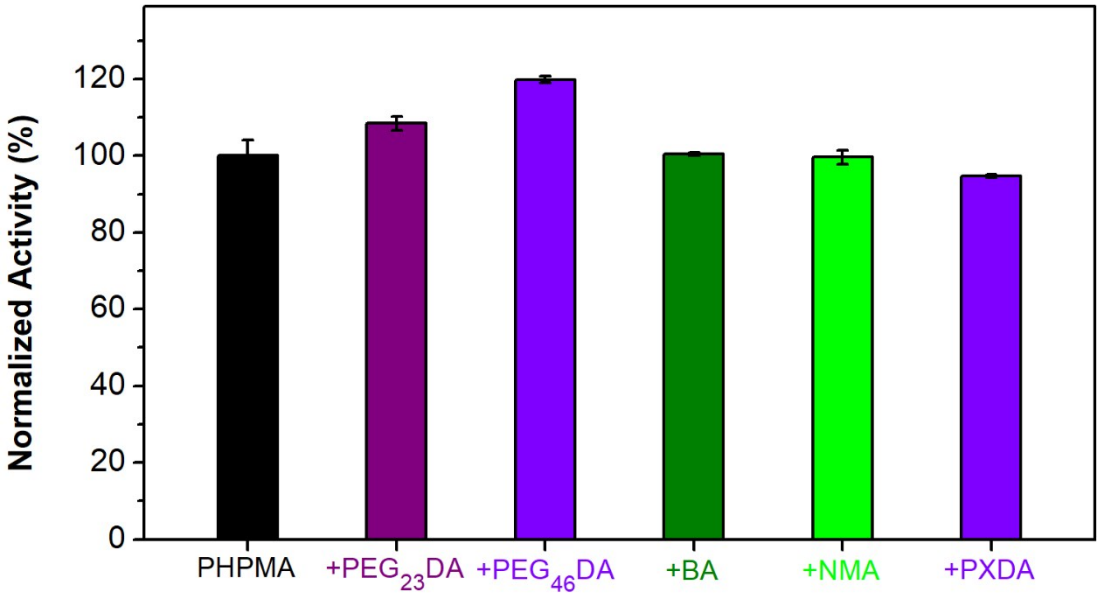

Figure S10. Control experiment comparing the activity of purified HRP-loaded PEG_{113}-*b*-$PHPMA_{400}$ vesicles before and after incubation with a series of primary amine and diamine molecules at room temperature for 18 hours in DI water, as determined at the end point of the colorimetric assay (end point = 30 min, λ = 492 nm), showing no negative effect of utilized amines on the HRP catalytic activity.

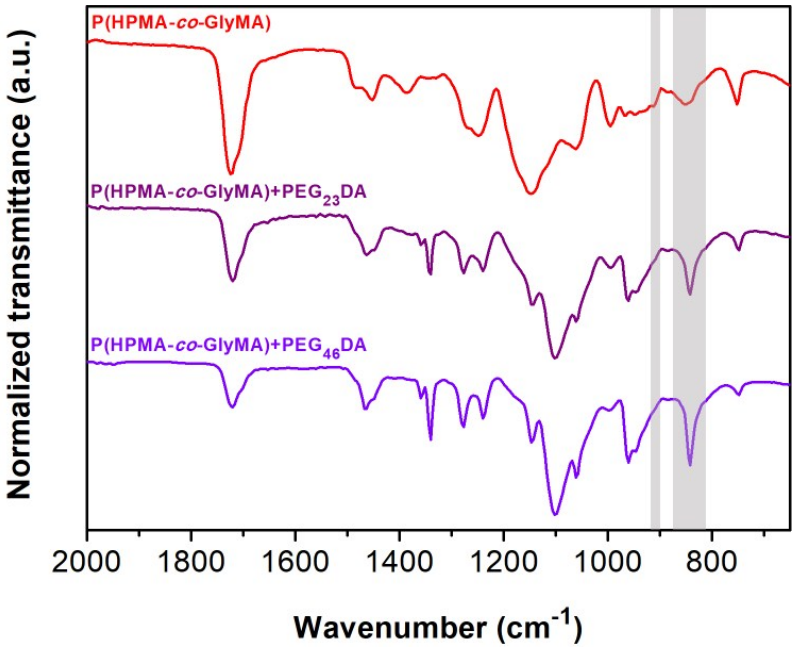

Figure S11. FT-IR spectra recorded for PEG_{113}-*b*-P($HPMA_{320}$-*co*-$GlyMA_{80}$) vesicles prior to membrane functionalization, and cross-linked PEG_{113}-*b*-P($HPMA_{320}$-*co*-$GlyMA_{80}$)+PEG_nDA vesicles showing the disappearance of the characteristic asymmetric vibration peaks of PGlyMA epoxy groups at 849 and 909 cm^{-1} after ring-opening reactions using PEG_nDA (n = 23, 46).

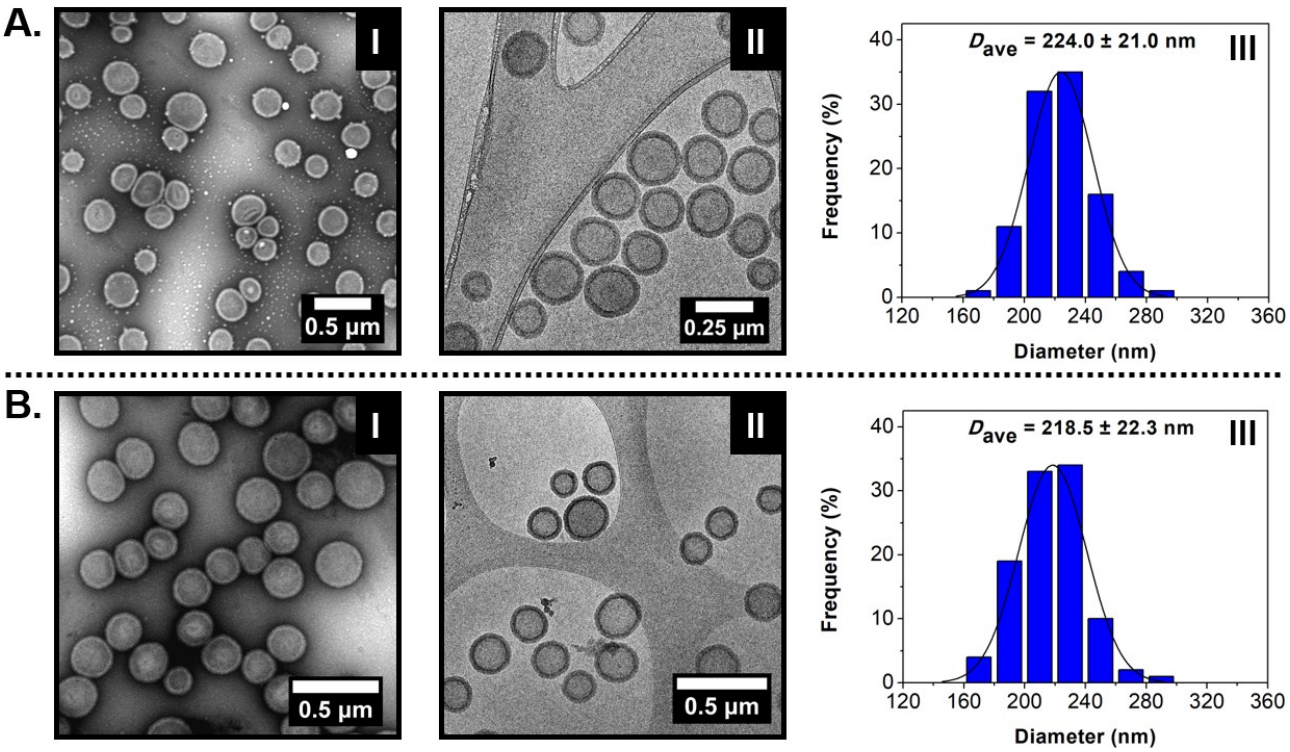

Figure S12. (A) For cross-linked HRP-loaded PEG_{113}-*b*-P($HPMA_{320}$-*co*-$GlyMA_{80}$)+$PEG_{23}DA$ vesicles, and (B) for cross-linked HRP-loaded PEG_{113}-*b*-P($HPMA_{320}$-*co*-$GlyMA_{80}$)+$PEG_{46}DA$ vesicles: (I) Representative dry-state TEM images, stained with 1 wt% UA solution, (II) representative cryo-TEM images, and (III) histograms of size distribution along with calculated average diameter values measured from particle analysis based on cryo-TEM images. In each case, at least 100 particles were analysed.

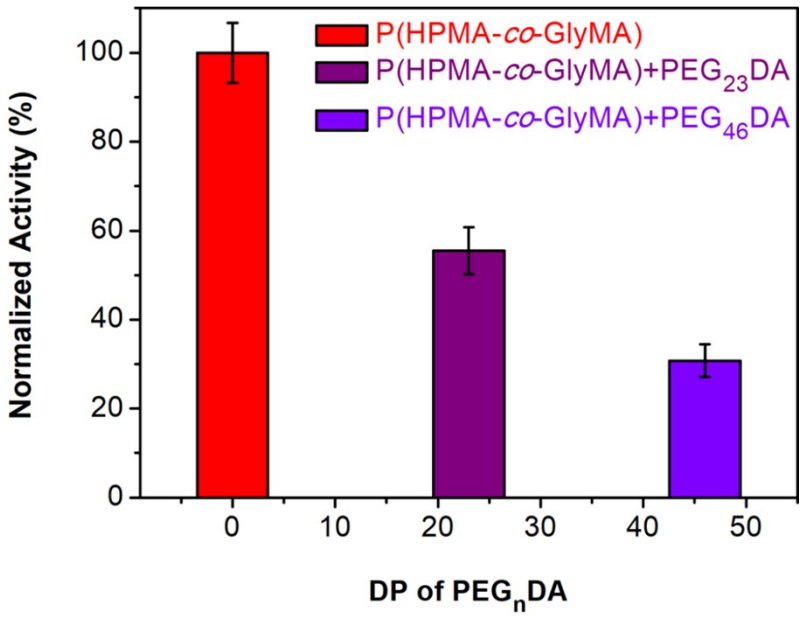

Figure S13. Normalized activities of PEG_nDA (n = 23, 46) cross-linked HRP-loaded PEG_{113}-*b*-P($HPMA_{320}$-*co*-$GlyMA_{80}$) vesicles compared to non-functionalized HRP-loaded PEG_{113}-*b*-P($HPMA_{320}$-*co*-$GlyMA_{80}$) vesicles at the end point of the enzymatic assay (end point = 30 min, λ = 492 nm), showing activity decrease upon increasing length of PEG_nDA (error bars show the standard deviation from four repeat measurements).

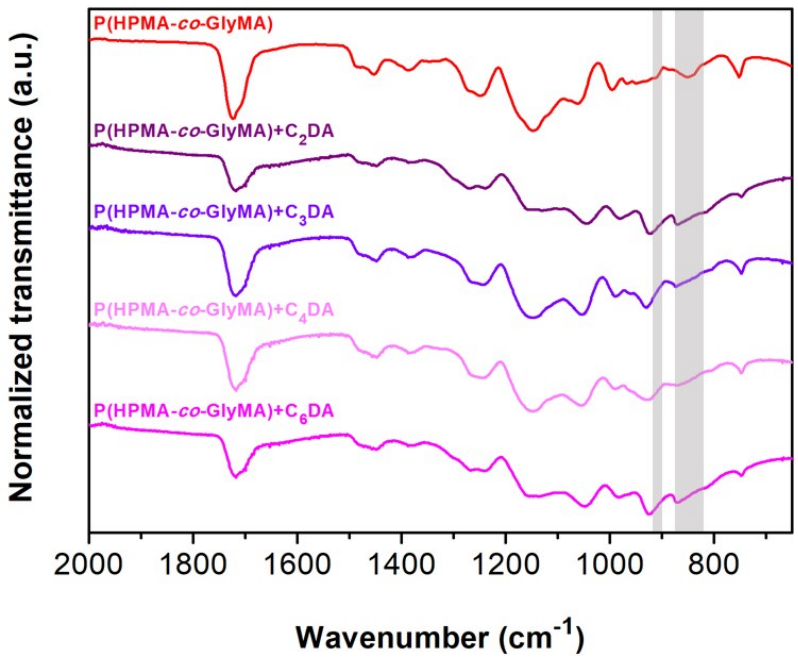

Figure S14. FT-IR spectra recorded for PEG_{113}-*b*-P($HPMA_{320}$-*co*-$GlyMA_{80}$) vesicles prior to membrane functionalization, and cross-linked PEG_{113}-*b*-P($HPMA_{320}$-*co*-$GlyMA_{80}$)+C_nDA vesicles showing the disappearance of the characteristic asymmetric vibration peaks of PGlyMA epoxy groups at 849 and 909 cm^{-1} after ring-opening reactions using C_nDA (n = 2-4, 6).

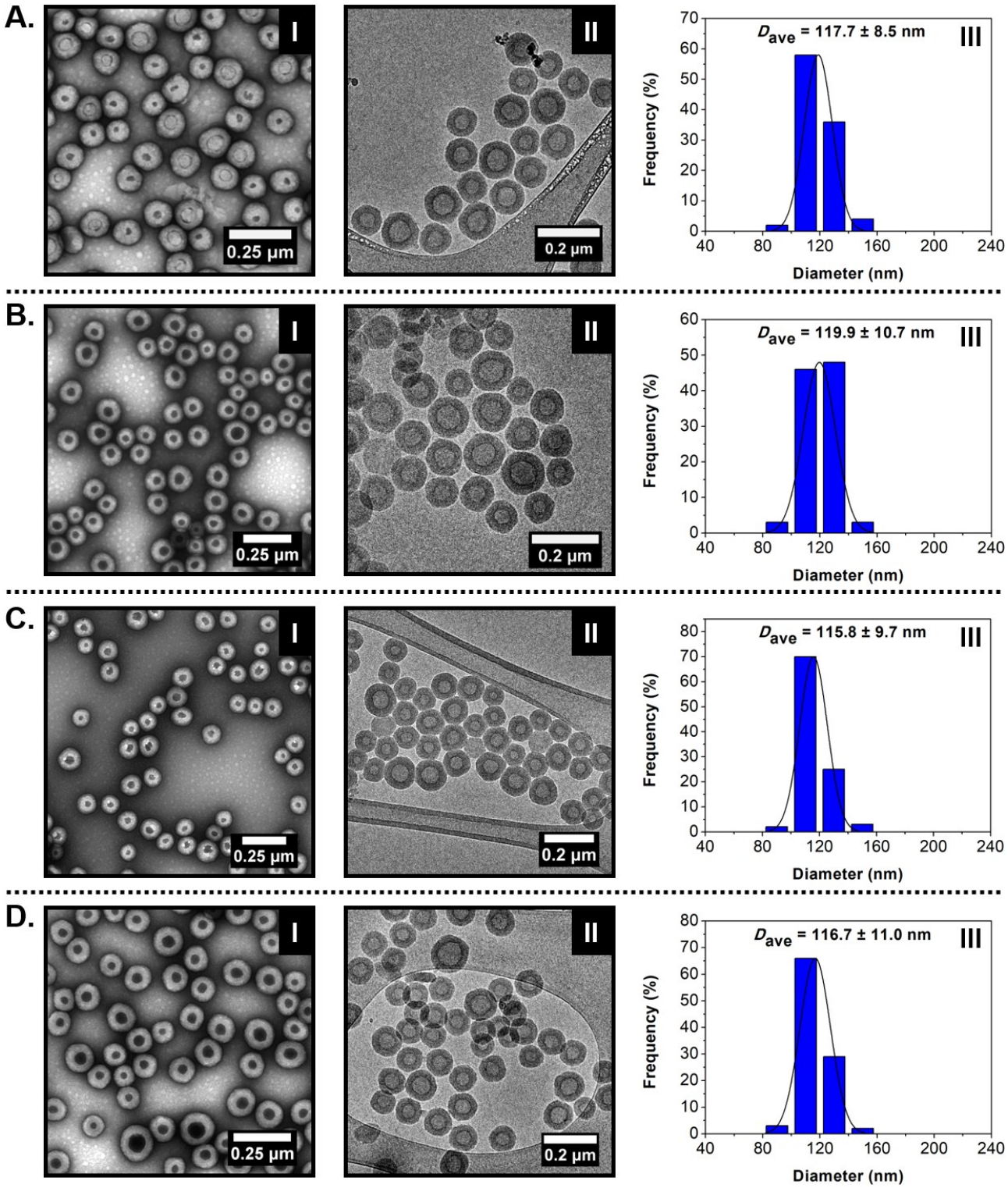

Figure S15. (A) For cross-linked HRP-loaded PEG_{113}-*b*-P($HPMA_{320}$-*co*-$GlyMA_{80}$)+C_2DA vesicles, (B) for cross-linked HRP-loaded PEG_{113}-*b*-P($HPMA_{320}$-*co*-$GlyMA_{80}$)+C_3DA vesicles, (C) for cross-linked HRP-loaded PEG_{113}-*b*-P($HPMA_{320}$-*co*-$GlyMA_{80}$)+C_4DA vesicles and (D) for cross-linked HRP-loaded

PEG_{113}-*b*-P($HPMA_{320}$-*co*-$GlyMA_{80}$)+C_6DA vesicles: (I) Representative dry-state TEM images, stained with 1 wt% UA solution, (II) representative cryo-TEM images, and (III) histograms of size distribution along with calculated average diameter values measured from particle analysis based on cryo-TEM images. In each case, at least 100 particles were analysed.

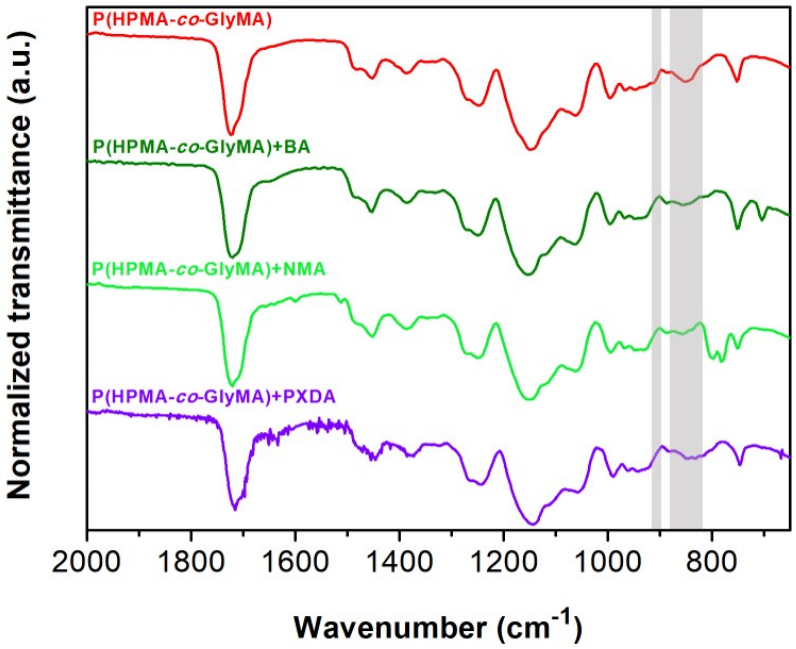

Figure S16. FT-IR spectra recorded for PEG_{113}-*b*-P($HPMA_{320}$-*co*-$GlyMA_{80}$) vesicles prior to membrane functionalization, BA/NMA-functionalized PEG_{113}-*b*-P($HPMA_{320}$-*co*-$GlyMA_{80}$) vesicles, and PXDA cross-linked PEG_{113}-*b*-P($HPMA_{320}$-*co*-$GlyMA_{80}$) vesicles showing the disappearance of the characteristic asymmetric vibration peaks of PGlyMA epoxy groups at 849 and 909 cm^{-1} after ring-opening reactions using BA, NMA or PXDA.

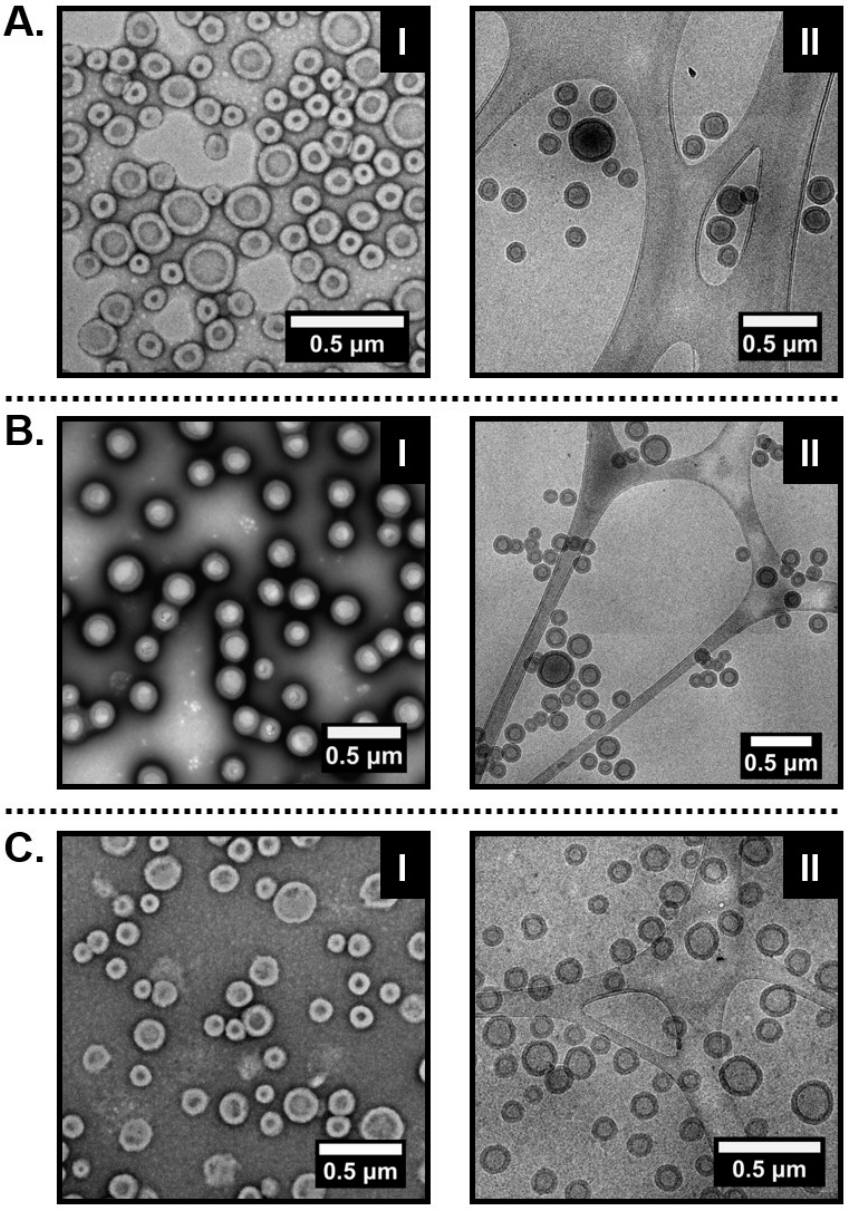

Figure S17. (A) For HRP-loaded PEG_{113}-*b*-P($HPMA_{320}$-*co*-$GlyMA_{80}$)+BA vesicles, (B) for HRP-loaded PEG_{113}-*b*-P($HPMA_{320}$-*co*-$GlyMA_{80}$)+NMA vesicles, and (C) for cross-linked HRP-loaded PEG_{113}-*b*-P($HPMA_{320}$-*co*-$GlyMA_{80}$)+PXDA vesicles: (I) Representative dry-state TEM images, stained with 1 wt% UA solution, and (II) representative cryo-TEM images.

Table S2. Summary of size, PD, and membrane thickness values for empty PEG_{113}-*b*-P($HPMA_{320}$-*co*-$GlyMA_{80}$) vesicles (*), and HRP-loaded PEG_{113}-*b*-P($HPMA_{320}$-*co*-$GlyMA_{80}$) vesicles before and after membrane functionalization using a series of primary amines, as determined by DLS analysis and TEM imaging, respectively.

Amine	D_h[a] (nm)	PD[a]	$D_{dry\text{-}state}$[b] (nm)	D_{cryo}[c] (nm)	M_{ave}[c] (nm)
-(*)	188.3 ± 5.6	0.18 ± 0.02	170.3 ± 23.0	175.5 ± 24.1	28.0 ± 3.0
-	182.6 ± 2.5	0.14 ± 0.04	171.9 ± 17.8	172.5 ± 25.5	27.9 ± 2.6
$PEG_{23}DA$	239.6 ± 6.4	0.11 ± 0.01	229.5 ± 33.2	224.0 ± 21.0	31.7 ± 2.4
$PEG_{46}DA$	238.4 ± 6.4	0.14 ± 0.04	233.3 ± 32.3	218.5 ± 22.3	31.8 ± 2.5
C_2DA	128.4 ± 3.8	0.13 ± 0.01	122.7 ± 8.3	117.7 ± 8.5	30.5 ± 2.1
C_3DA	123.8 ± 0.6	0.12 ± 0.02	122.2 ± 9.9	119.9 ± 10.7	30.1 ± 2.2
C_4DA	1497 ± 266	0.24 ± 0.04	122.3 ± 8.9	115.8 ± 9.7	31.6 ± 2.3
C_6DA	1389 ± 149	0.23 ± 0.06	123.1 ± 10.1	116.7 ± 11.0	30.7 ± 2.0
PXDA	203.4 ± 1.9	0.06 ± 0.01	181.3 ± 22.9	172.7 ± 16.4	31.1 ± 2.7
BA	203.4 ± 2.8	0.08 ± 0.02	164.6 ± 26.8	175.4 ± 27.7	33.2 ± 2.9
NMA	204.0 ± 4.7	0.02 ± 0.01	190.7 ± 16.2	182.5 ± 18.9	37.6 ± 2.8
AMA	*Macroscopic precipitation – unstable particles*				

[a]D_h and PD values measured from DLS analysis. [b]Average diameter values measured from particle analysis based on dry-state TEM images. [c]Average diameter and membrane thickness values measured from particle analysis based on cryo-TEM images. In each case, at least 100 particles were analyzed.

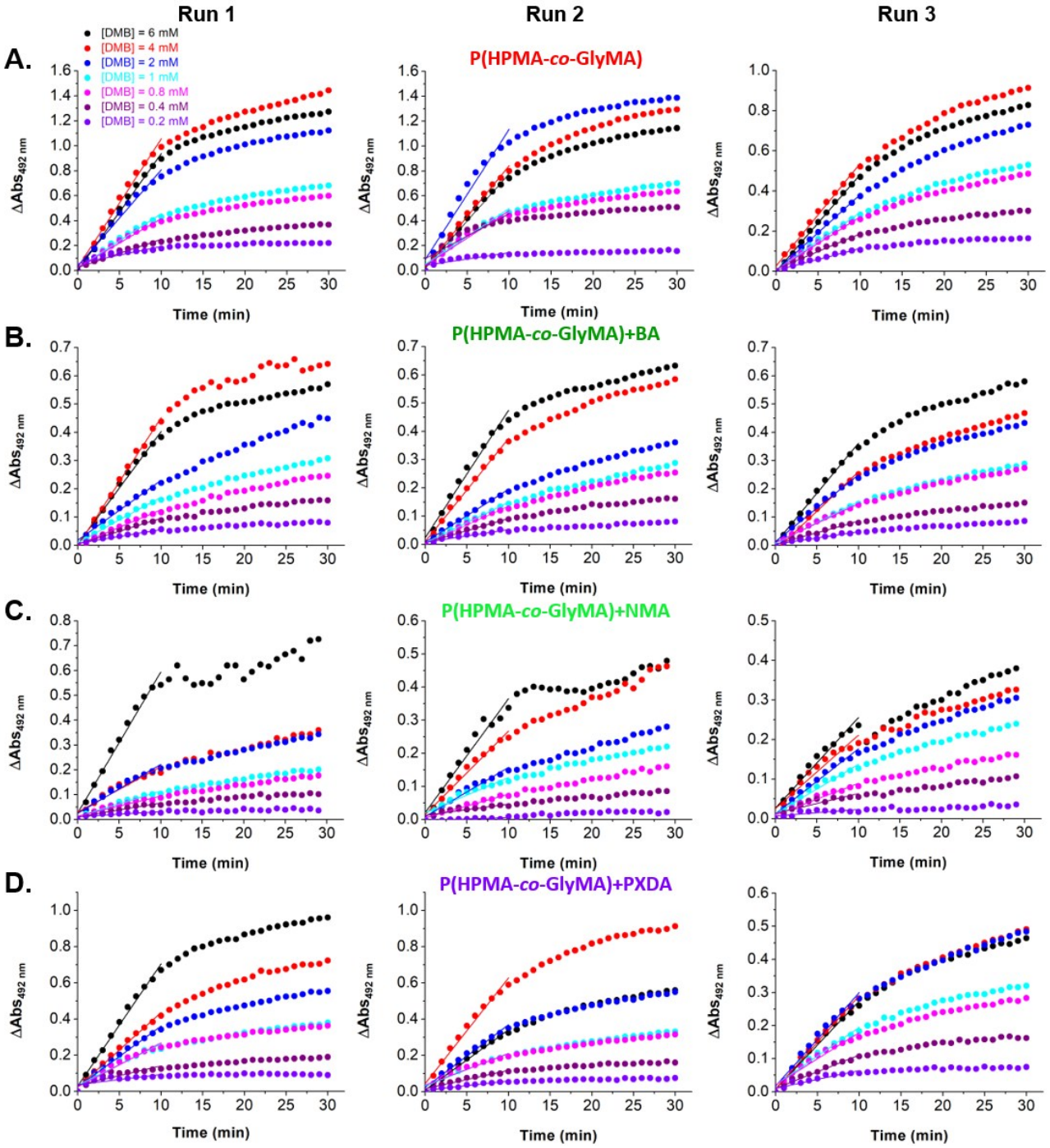

Figure S18. Enzymatic activity of (A) HRP-loaded PEG_{113}-*b*-P($HPMA_{320}$-*co*-$GlyMA_{80}$) vesicles, (B) HRP-loaded PEG_{113}-*b*-P($HPMA_{320}$-*co*-$GlyMA_{80}$)+BA vesicles, (C) HRP-loaded PEG_{113}-*b*-P($HPMA_{320}$-*co*-$GlyMA_{80}$)+NMA vesicles, and (D) HRP-loaded PEG_{113}-*b*-P($HPMA_{320}$-*co*-$GlyMA_{80}$)+PXDA vesicles at different [DMB] (with [H_2O_2] under saturating conditions) (end point = 30 min, λ = 492 nm). In each case, the average initial slope of three repeat measurements (V_0) for the first 10 min of the assay was used for construction of Michaelis-Menten kinetic plots and was normalized against V_{max}.

Table S3. Summary of enzyme activity curve fitting analysis for HRP-loaded PEG_{113}-*b*-P($HPMA_{320}$-*co*-$GlyMA_{80}$) and HRP-loaded PEG_{113}-*b*-P($HPMA_{320}$-*co*-$GlyMA_{80}$)+BA/NMA/PXDA vesicles utilized for construction of Michaelis-Menten kinetic plots.

Sample	[DMB] (mM)	Slope Run 1	Slope Run 2	Slope Run 3	Average Slope	Standard Deviation
PEG_{113}-*b*-P($HPMA_{320}$-*co*-$GlyMA_{80}$)	6	0.0938	0.0760	0.0481	0.0726	0.0188
	4	0.1031	0.0817	0.0511	0.0786	0.0214
	2	0.0774	0.1046	0.0378	0.0733	0.0274
	1	0.0435	0.0448	0.0284	0.0389	0.0074
	0.8	0.0392	0.0438	0.0263	0.0364	0.0074
	0.4	0.0227	0.0360	0.0176	0.0254	0.0077
	0.2	0.0138	0.0103	0.0109	0.0116	0.0015
PEG_{113}-*b*-P($HPMA_{320}$-*co*-$GlyMA_{80}$)+BA	6	0.0398	0.0450	0.0354	0.0401	0.0039
	4	0.0453	0.0365	0.0279	0.0366	0.0071
	2	0.0212	0.0186	0.0237	0.0212	0.0020
	1	0.0161	0.0143	0.0147	0.0150	0.0008
	0.8	0.0124	0.0133	0.0137	0.0132	0.0005
	0.4	0.0091	0.0086	0.0082	0.0086	0.0004
	0.2	0.0049	0.0045	0.0045	0.0046	0.0002
PEG_{113}-*b*-P($HPMA_{320}$-*co*-$GlyMA_{80}$)+NMA	6	0.0568	0.0344	0.0229	0.0380	0.0141
	4	0.0183	0.0252	0.0186	0.0207	0.0031
	2	0.0197	0.0149	0.0165	0.0170	0.0020
	1	0.0102	0.0106	0.0125	0.0111	0.0010
	0.8	0.0082	0.0072	0.0080	0.0078	0.0004
	0.4	0.0057	0.0034	0.0050	0.0047	0.0009
	0.2	0.0020	0.0009	0.0017	0.0015	0.0005
PEG_{113}-*b*-P($HPMA_{320}$-*co*-$GlyMA_{80}$)+PXDA	6	0.0676	0.0333	0.0266	0.0425	0.0180
	4	0.0413	0.0583	0.0282	0.0426	0.0124
	2	0.0335	0.0346	0.0282	0.0321	0.0028
	1	0.0229	0.0181	0.0173	0.0195	0.0024
	0.8	0.0243	0.0175	0.0158	0.0192	0.0037
	0.4	0.0107	0.0102	0.0010	0.0073	0.0045
	0.2	0.0057	0.0051	0.0054	0.0054	0.0002